

Microscopic Superfluidity in Bose Gases: From 3D to 1D

Kwangsik Nho¹ and D. Blume¹

¹*Department of Physics and Astronomy, Washington State University, Pullman, Washington 99164-2814, USA*

The superfluid fraction of ideal and interacting inhomogeneous Bose gases with varying asymmetry is investigated at finite temperature using well-known properties of the harmonic oscillator as well as the essentially exact microscopic path integral Monte Carlo method. We find that the superfluid fraction (i) is essentially independent of the interaction strength for all temperatures considered, (ii) changes profoundly as the effective dimensionality is varied from three- to one-dimensional, (iii) is approximately equal to the condensate fraction N_0/N for spherical Bose gases, and (iv) deviates dramatically from N_0/N for highly-elongated Bose gases.

Macroscopic objects such as liquid ⁴He show many peculiar properties that can be attributed to superfluidity [1]. Among these are the absence of viscosity, the occurrence of persistent currents, the existence of vortices and the reduction of the moment of inertia. Connections between manifestations of superfluidity and Bose Einstein condensation have been studied extensively in the context of liquid ⁴He since the discovery of its superfluidity in 1938. While much progress has been made in our understanding of such strongly interacting systems, many questions remain unanswered.

Thanks to the realization of gaseous Bose Einstein condensates in 1995 [2], the study of superfluid effects of mesoscopic systems has become possible. Indeed, the creation of vortices [3] and vortex lattices [4] has been demonstrated in inhomogeneous Bose gases, and, most recently, also in degenerate Fermi gases in the BEC-BCS crossover regime [5]. Following the work on ⁴He enclosed in a cylinder [6], superfluidity of inhomogeneous systems can be described through their rotational properties. The superfluid fraction is defined by the departure of the quantum mechanical moment of inertia $\Theta_{\hat{n}}$ with respect to \hat{n} from its classical, or rigid, value $\Theta_{\hat{n}}^{rig}$. Here, the moment of inertia $\Theta_{\hat{n}}$, $\Theta_{\hat{n}} = (\partial \langle \vec{L} \cdot \hat{n} \rangle_{\omega} / \partial \omega)_{\omega=0}$, is defined by the linear response of the system to a rotational field $H_{ext} = -\vec{\omega} \cdot \vec{L}$, where $\vec{\omega} = \omega \hat{n}$; ω denotes the angular frequency and \vec{L} the total angular momentum. The thermal expectation value $\langle \cdot \rangle_{\omega}$ is evaluated for the system perturbed by H_{ext} . The normal fraction is the part of the system that responds classically, i.e., $\Theta_{\hat{n}} / \Theta_{\hat{n}}^{rig}$, and the superfluid fraction $(n_s/n)_{\hat{n}}$ is $1 - \Theta_{\hat{n}} / \Theta_{\hat{n}}^{rig}$.

The temperature dependence of $\Theta_{\hat{n}}$ has been evaluated for a non-interacting Bose gas under harmonic confinement in the so-called macroscopic approximation [7]. The effects of weak interactions have been estimated within the Thomas-Fermi approximation [7]. This Letter determines the temperature-dependence of $\Theta_{\hat{n}}$ and $\Theta_{\hat{n}}^{rig}$, and hence of the superfluid fraction, for small atomic gases with $N = 27$ bosons for varying confinement and interaction strength non-perturbatively using the essentially exact microscopic path integral Monte Carlo (PIMC) method [8]. For the ideal gas, we additionally determine thermal expectation values using well-known prop-

erties of the harmonic oscillator [9]. In contrast to ⁴He clusters [10] or deformed nuclei [11], whose interaction strength and internal temperature are largely “set by nature”, atomic gases provide us with unprecedented control. The temperature can be controlled by changing the cooling scheme [12], the interaction strength can be tuned by applying an external magnetic field in the vicinity of a Feshbach resonance [13, 14], and the dimensionality can be reduced by varying the external confinement [15, 16]. Here, we focus on the crossover from three-dimensional (3D) to one-dimensional (1D) behavior. We show that reduced dimensionality leads to an increase of the superfluid response. The superfluid fraction for 3D gases roughly coincides with the condensate fraction N_0/N . In the quasi-1D regime, however, the superfluid fraction is much larger than N_0/N . Our calculations show that the superfluid response depends, if at all, weakly on the strength of the atom-atom interactions.

Consider N bosons with mass m under external harmonic confinement,

$$H = \sum_{j=1}^N \left[\frac{-\hbar^2}{2m} \nabla_j^2 + \frac{1}{2} m (\omega_{\rho}^2 \rho_j^2 + \omega_z^2 z_j^2) \right] + \sum_{j < k}^N V(r_{jk}). \quad (1)$$

Here, ρ_j and z_j denote the transverse and longitudinal coordinate of the j th atom, respectively, and ω_{ρ} and ω_z the transverse and longitudinal angular frequency of the trapping potential, respectively. The atom-atom potential V depends on the interparticle distance r_{jk} between atom j and atom k . For the non-interacting gas, i.e., $V(r) = 0$, we calculate thermal expectation values in the grandcanonical ensemble using well-known properties of the harmonic oscillator [9]. To simulate effectively repulsive Bose gases, we use a hard sphere potential $V(r)$ with 3D atom-atom scattering length a ; in particular, $a = 0.00433$ and $0.0433a_z$, where $a_z = \sqrt{\hbar/(m\omega_z)}$. In this case, we use the numerically more involved PIMC technique [8], which determines thermal expectation values in the canonical ensemble. For the purpose of the present study, differences between expectation values calculated in the grandcanonical and in the canonical ensemble (see also Ref. [17]) are negligible.

To investigate the crossover from 3D to 1D for N bosons, we vary the angular frequency ω_{ρ} such that

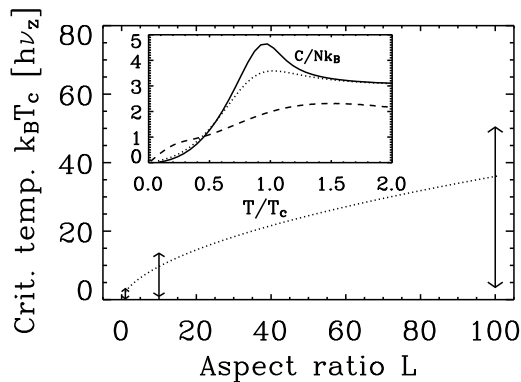


FIG. 1: Approximate 3D transition temperature $k_B T_c$ (see, e.g., Eq. (19) of Ref. [18]) in units of $\hbar\omega_z$ ($\omega_z = 2\pi\nu_z$) as a function of L for $N = 27$. Vertical arrows indicate the interval $0.1 \leq T/T_c \leq 1.4$ for $L = 1, 10$ and 100 . The inset shows the specific heat C divided by Nk_B calculated in the grandcanonical ensemble as a function of T/T_c for $N = 27$ and $L = 1$ (solid line), 10 (dotted line) and 100 (dashed line).

$L = 1, 10$ and 100 , where $L = \omega_\rho/\omega_z$. The approximate 3D transition temperature T_c , obtained for vanishing atom-atom interactions, then depends on ω_ρ , ω_z and N (the T_c used throughout this paper includes finite-size corrections; see, e.g., Eq. (19) of Ref. [18]). A dotted line in Fig. 1 shows T_c as a function of the aspect ratio L for $N = 27$. Below, we report calculations for $L = 1, 10$ and 100 over a wide temperature range, i.e., $0.1 \lesssim T/T_c \lesssim 1.4$ (see vertical arrows in Fig. 1).

Highly-elongated gases at $T = 0$ can to a very good approximation be described by an effective 1D Hamiltonian for any 3D scattering length a if $N/L \ll 1$ [19]. For $N = 27$ and $L = 100$, we find $N/L = 0.27$. At finite temperature, the behavior of highly-elongated Bose gases depends on two energy scales, the oscillator energies $\hbar\omega_\rho$ and $\hbar\omega_z$ of the tight and weak confinement direction, respectively. For $N = 27$ and $L = 100$, three temperature regimes exist [20]: i) T is larger than the 3D transition temperature T_c (excited transverse modes are occupied); ii) T is lower than T_c but larger than the 1D transition temperature T_c^{1D} [21] (transverse excitations are largely frozen out); and iii) T is smaller than T_c^{1D} (excited longitudinal modes are largely frozen out). For $N = 27$ and $L = 100$, the approximate 3D transition temperature is $k_B T_c = 36.0\hbar\omega_z$, while the approximate 1D transition temperature is $k_B T_c^{1D} = 9.67\hbar\omega_z$, corresponding to $0.269T_c$.

To understand the significance of the 3D transition temperature T_c we calculate the specific heat C , $C = (\partial U/\partial T)_N$, where U denotes the internal energy [20], for the ideal gas in the grandcanonical ensemble. The inset of Fig. 1 shows the specific heat C for $N = 27$ for three different aspect ratios, i.e., $L = 1$ (solid line), 10 (dotted line) and 100 (dashed line). Since the specific heat

shows a peak, although broadened due to the finite size of the Bose gas, at $T/T_c \approx 1$ for $L = 1$ and 10 , and at $T/T_c \approx 1.4$ for $L = 100$, it is justified to speak of a 3D transition temperature for Bose gases with as few as $N = 27$ atoms. In contrast, the transition to macroscopic occupation of the lowest energy state for the quasi-1D gas with $L = 100$, i.e., to “1D condensation”, does not imprint a clear signature on the specific heat (see also Ref. [20, 21]).

Figure 2 shows the expectation value of $|z|$ in units of

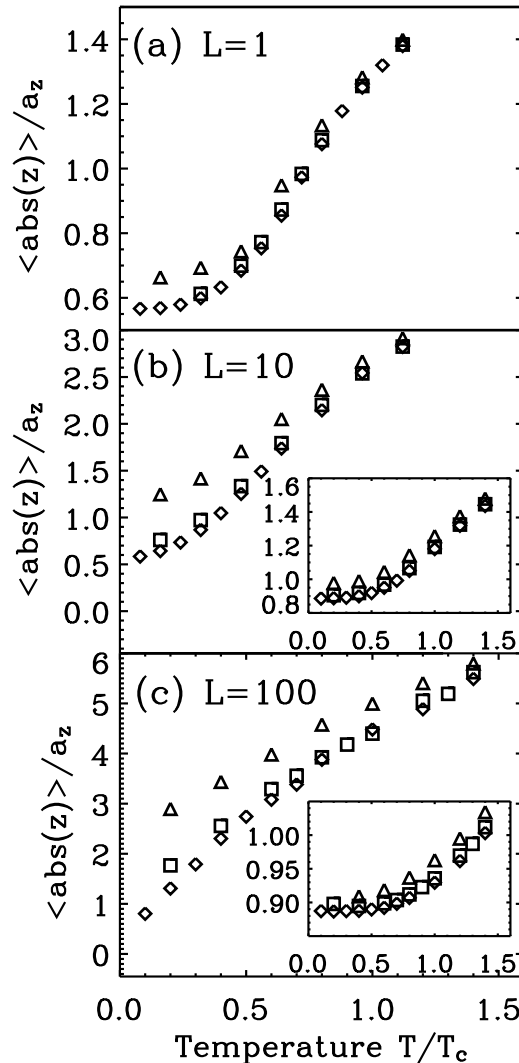


FIG. 2: PIMC expectation value of $|z|$ in units of a_z as a function of T/T_c for $N = 27$ for (a) $L = 1$, (b) 10 and (c) 100 . Diamonds show the results for $a/a_z = 0$, squares those for $a/a_z = 0.00433$ and triangles those for $a/a_z = 0.0433$. For $L = 10$ and $L = 100$, the insets show the expectation value of ρ in units of a_ρ as a function of T/T_c . Statistical uncertainties are smaller than the symbol size [22].

a_z , calculated using the PIMC method, as a function of

the scaled temperature T/T_c for (a) $L = 1$, (b) $L = 10$ and (c) $L = 100$ for three scattering lengths; $a = 0$ (diamonds), $a = 0.00433a_z$ (squares) and $a = 0.0433a_z$ (triangles). At low T/T_c , our expectation values of $|z|$ for $a = 0$ (circles) approach the zero temperature value, i.e., $\langle |z| \rangle = 0.564a_z$. Since the energy of the transverse excitations increases with increasing L , the expectation value of $|z|$ for $L = 100$ approaches the zero-temperature value at a lower scaled temperature T/T_c than that for $L = 1$. For repulsive interactions, i.e., $a/a_z = 0.00433$ (squares) and $a/a_z = 0.0433$ (triangles), the expectation value of $|z|$ increases compared to that of the non-interacting gas.

The insets of Figs. 2(b) and (c) show the expectation value of ρ in units of a_ρ , where $a_\rho = \sqrt{\hbar/(m\omega_\rho)}$, for $L = 10$ and 100, respectively, as a function of T/T_c (using the same symbols as in the main figure). At $T = 0$, the expectation value of ρ is $0.886a_\rho$ for the non-interacting gas. Just as the expectation value of $|z|$, that of ρ depends strongly on the interaction strength a . The nearly constant expectation value of ρ for $L = 100$ (for a given value of a) at low T/T_c indicates that the excitations in the transverse direction are frozen out for $T \lesssim 0.4T_c$, and hence for $T < T_c^{1D}$.

We now turn to the calculation of the superfluid fraction $(n_s/n)_{\hat{n}}$ with respect to the axis \hat{n} . For the non-interacting gas, the superfluid fraction with respect to, e.g., the z -axis, can be calculated from the thermal expectation values of x^2 and y^2 [7]. To this aim, we consider a trapping geometry with $\omega_y = \omega_x + \Delta\omega$ in the limit $\Delta\omega \rightarrow 0$ (see Eq. (7) of Ref. [7]). Dotted lines in Fig. 3 show the resulting superfluid fraction $(n_s/n)_{\hat{z}}$, calculated in the grandcanonical ensemble, for (a) $L = 1$, (b) $L = 10$ and (c) $L = 100$ as a function of T/T_c for $N = 27$ non-interacting bosons.

Within the PIMC formulation, the superfluid fraction $(n_s/n)_{\hat{n}}$ can be calculated from the square of the projected area $A_{\hat{n}}$ [10], where $A_{\hat{n}} = \vec{A} \cdot \hat{n}$ and \vec{A} denotes the area enclosed by the imaginary time paths [8]. Symbols in Fig. 3 show the superfluid fraction $(n_s/n)_{\hat{z}}$ calculated using the PIMC method for three different aspect ratios L ; diamonds show our results for $a = 0$, squares those for $a = 0.00433a_z$, and triangles those for $a = 0.0433a_z$. For $a = 0$, the PIMC results for $(n_s/n)_{\hat{z}}$ (diamonds), calculated in the canonical ensemble, agree well with those calculated in the grandcanonical ensemble (dotted lines).

The superfluid fraction $(n_s/n)_{\hat{z}}$ is essentially one at small scaled temperatures, and decreases gradually with increasing T/T_c . For $L = 1$, $(n_s/n)_{\hat{z}}$ is about 0.05 for $T/T_c = 1$. For the larger aspect ratios [see Figs. 3(b) and (c)], in contrast, $(n_s/n)_{\hat{z}}$ is significantly larger at the transition temperature (about 0.2 for $L = 10$ and about 0.65 for $L = 100$). When plotted, as done here, as a function of T/T_c the superfluid fraction $(n_s/n)_{\hat{z}}$ shows a very weak, if any, dependence on the interaction strength for all aspect ratios.

The spherically symmetric system with $L = 1$ has no

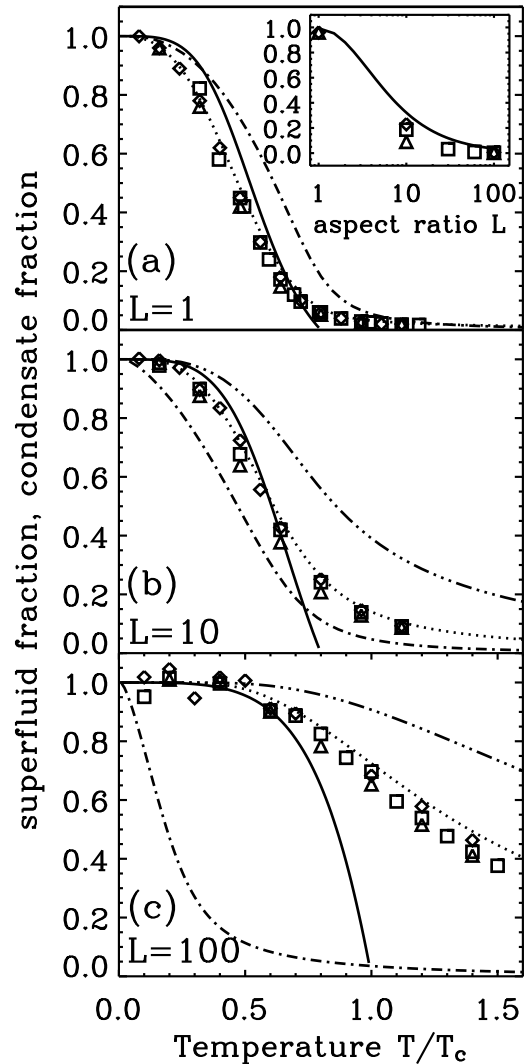


FIG. 3: Superfluid fraction $(n_s/n)_{\hat{z}}$ for $N = 27$ and (a) $L = 1$, (b) $L = 10$ and (c) $L = 100$: Diamonds show the PIMC results for $a/a_z = 0$, squares those for $a/a_z = 0.00433$ and triangles those for $a/a_z = 0.0433$ [23]; dotted lines show $(n_s/n)_{\hat{z}}$ for $a = 0$ calculated in the grandcanonical ensemble. Solid lines show the superfluid fraction given by Eq. (2). Dash-dotted lines show the condensate fraction N_0/N , and dot-dot-dot-dashed lines the fraction N_{1D}/N . The inset of panel (a) shows $(n_s/n)_{\hat{x}}$ for $N = 27$ and $T/T_c = 0.2$ for three different interaction strengths (using the same symbols as in the main figure) as a function of L on a logarithmic scale.

preferred symmetry axis, implying $(n_s/n)_{\hat{z}} = (n_s/n)_{\hat{x}}$. For $L > 1$, however, the superfluid fraction $(n_s/n)_{\hat{x}}$ is distinctly different from $(n_s/n)_{\hat{z}}$. Geometric arguments imply that $(n_s/n)_{\hat{x}}$ approaches zero when the system reaches the quasi-1D regime. When exposed to a rotation about \hat{x} , the atoms move with the external trap, thus implying $\Theta_{\hat{x}}^{rig} = \Theta_{\hat{x}}$. The inset of Fig. 3(a) shows the su-

perfluid fraction $(n_s/n)_{\hat{x}}$ for $N = 27$ and $T/T_c = 0.2$ for three different scattering lengths (using the same symbols as in the main figure) as a function of the aspect ratio L . It is evident that $(n_s/n)_{\hat{x}}$ decreases rapidly with increasing L .

To connect with earlier work, we consider an analytical expression for the superfluid fraction $(n_s/n)_{\hat{z}}$, which has been derived using the semi-classical approximation for the non-interacting gas [7]. For a trap geometry with $\omega_y \approx \omega_x$ and $\omega_z = \omega_x/L$, we generalize the treatment by Stringari [7] to account for rotations about $\hat{n} = \hat{x}$. To additionally improve the accuracy for small N , we use the T_c that accounts for finite-size effects (see above),

$$(n_s/n)_{\hat{n}} = \frac{A \left[1 - (T/T_c)^3 \right]}{1 - \left(\frac{T}{T_c} \right)^3 + B \frac{1.80079}{L} \left(\frac{T}{T_c} \right)^4 \frac{k_B T_c}{\hbar \omega_z}}. \quad (2)$$

Here, A and B denote constants depending on the geometry of the trap; $A = B = 1$ for $\hat{n} = \hat{z}$, and $A = 1 - [(1-L)/(1+L)]^2$ and $B = (L^2 + 1)/(L + 1)$ for $\hat{n} = \hat{x}$. Solid lines in Fig. 3 show the resulting approximate superfluid fractions $(n_s/n)_{\hat{z}}$ (main figure) and $(n_s/n)_{\hat{x}}$ [inset of Fig. 3(a)]. The agreement between Eq. (2) and our numerical results for $L = 1$ is good. For $L = 100$, however, Eq. (2) describes the superfluid fraction only qualitatively. In particular, Eq. (2) clearly underestimates $(n_s/n)_{\hat{z}}$ for $T/T_c \gtrsim 1$.

For comparison, dash-dotted lines in Fig. 3 show the condensate fraction N_0/N calculated in the grandcanonical ensemble for the non-interacting gas. For $L = 1$, the condensate fraction roughly agrees with the superfluid fraction. For $L = 100$, in contrast, N_0/N drops to zero at much lower temperatures than $(n_s/n)_{\hat{z}}$. This shows that the condensate fraction and the superfluid fraction are distinctly different quantities for highly-elongated systems. For comparison, dot-dot-dot-dashed lines show the fraction of atoms N_{1D}/N in the lowest transverse mode, where $N_{1D} = \sum_k N_{00k}$ and N_{ijk}/N denotes the fraction of atoms in the state with i quanta in the x -, j quanta in the y - and k quanta in the z -direction. For the highly-elongated gas with $L = 100$, the fraction of atoms N_{1D}/N is larger than the superfluid fraction $(n_s/n)_{\hat{z}}$ but shows a similar overall behavior. Calculations for the non-interacting gas for $N = 1000$ and $L = 5000$ (not shown) indicate similar behaviors.

In summary, this Letter describes microscopic calculations for small Bose gases over a wide temperature range. We study the crossover from 3D to 1D by changing the trapping frequency. Since all our calculations are performed in full $3N$ -dimensional configuration space, the freezing of the radial motion at low temperatures emerges from our calculations; it is not an input. Specifically, we determine the temperature dependence of the quantum mechanical moment of inertia. This quantity has played a key role in the study of finite-size bosonic he-

lium droplets over the past 10 years or so [24]. Measurements of the quantum mechanical moment of inertia of an impurity embedded inside such a droplet have, e.g., shown unambiguously that bosonic helium clusters with as few as about 60 atoms are superfluid [25]. This paper shows that the effects of superfluidity are altered as the effective dimensionality of the trapped gas changes from 3D to 1D. The superfluid fraction $(n_s/n)_{\hat{z}}$ is enhanced as the dimensionality is reduced. In the quasi-1D regime, the superfluid response is distinctly different from the condensate fraction N_0/N and very roughly follows the fraction N_{1D}/N of atoms in the lowest transverse mode.

We gratefully acknowledge fruitful discussions with S. Giorgini and support by the NSF, grant PHY-0331529.

-
- [1] R. J. Donnelly, *Quantized Vortices in Helium II* (Cambridge University Press, Cambridge, 1995).
 - [2] M. H. Anderson *et al.*, *Science* **269**, 198 (1995).
 - [3] M. R. Matthews *et al.*, *Phys. Rev. Lett.* **83**, 2498 (1999).
 - [4] J. R. Abo-Shaer, C. Raman, J. M. Vogels and W. Ketterle, *Science* **292**, 476 (2001).
 - [5] M. Zwierlein, Talk at workshop on ‘‘Strongly Interacting Quantum Gases’’; April 18-21, 2005; Ohio Center for Theoretical Science.
 - [6] G. Baym, in *Mathematical Methods in Solid State and Superfluid Theory*, edited by R. C. Clark and E. H. Derrick (Oliver and Boyd, Edinburgh, 1969).
 - [7] S. Stringari, *Phys. Rev. Lett.* **76**, 1405 (1996).
 - [8] D. M. Ceperley, *Rev. Mod. Phys.* **67**, 279 (1995).
 - [9] S. R. de Groot, G. J. Hooyman and A. Seldam, *Proc. R. Soc. London, Ser. A* **203**, 266 (1950).
 - [10] P. Sindzingre, M. L. Klein and D. M. Ceperley, *Phys. Rev. Lett.* **63**, 1601 (1989).
 - [11] A. Bohr and B. R. Mottelson, *Nuclear Structure, Volume II, Nuclear Deformations* (W. A. Benjamin, Inc., Reading, 1975).
 - [12] F. Gerbier *et al.*, *Phys. Rev. Lett.* **92**, 030405 (2004).
 - [13] S. Inouye *et al.*, *Nature* **392**, 151 (1998).
 - [14] S. L. Cornish *et al.*, *Phys. Rev. Lett.* **85**, 1795 (2000).
 - [15] A. Görlitz *et al.*, *Phys. Rev. Lett.* **87**, 130402 (2001).
 - [16] M. Greiner *et al.*, *Phys. Rev. Lett.* **87**, 160405 (2001).
 - [17] C. Herzog and M. Olshanii, *Phys. Rev. A* **55**, 3254 (1997).
 - [18] F. Dalfovo, S. Giorgini, L. P. Pitaevskii and S. Stringari, *Rev. Mod. Phys.* **71**, 463 (1999).
 - [19] see, e.g., D. S. Petrov, D. M. Gangardt and G. V. Shlyapnikov, *J. Phys. IV (France)* **116**, 3 (2004).
 - [20] N. J. van Druten and W. Ketterle, *Phys. Rev. Lett.* **79**, 549 (1997).
 - [21] W. Ketterle and N. J. van Druten, *Phys. Rev. A* **54**, 656 (1996).
 - [22] Expectation values calculated by the PIMC method have an errorbar since the technique is stochastic in nature.
 - [23] The PIMC data for small T/T_c have the largest errorbars, the largest of which is at most four times the symbol size.
 - [24] J. P. Toennies, A. V. Vilesov and K. B. Whaley, *Phys. Today* **54**, 31 (2001).
 - [25] S. Grebenev, J. P. Toennies and A. F. Vilesov, *Science*

279, 2083 (1998).